GENERAL ELECTRIC COMPOSITE RING-DISK FLYWHEEL: RECENT AND POTENTIAL DEVELOPMENTS

Anthony P. Coppa
General Electric Company
Space Systems Division
Philadelphia, Pennsylvania

INTRODUCTION

During the past few years, an increasing recognition has developed of the important benefits that can be gained by utilizing high performance flywheel systems in spacecraft. While the case for flywheels for spacecraft power and combined power/attitude control was fairly well established by the 1974 NASA/Rockwell Study (Refs. 1-2), a more solid acceptance of it was inhibited by the then current state of technology, among other reasons. One of the key factors supporting the case for flywheels was (and is) the composite rotor, with its potential for very high density and manageable containment. Although flywheel systems incorporating then available metallic rotors appeared to be competitive with electrochemical energy storage systems for certain missions, a limited potential, certainly for long term performance growth, and an unresolved containment issue undoubtedly dampened significant system development.

The situation has, however, changed for the better in recent years due to important developments in composite rotor technology which have proceeded from the mechanical energy storage technology (MEST) program sponsored by the U.S. Department of Energy (DOE) and conducted by the Lawrence Livermore National Laboratory (LLNL). The primary objective of the program was to develop by 1984 an economical and practical composite flywheel having an energy density of 88 Wh/kg at failure with an operational range of 44-55 Wh/kg and an energy storage capacity of approximately 1 kWh. In addition, concerns regarding safety dictated the development of flywheel containment technology.

Initially, the DOE/LLNL program sponsored the development of 10 different composite rotor designs. Considerable data regarding the dynamics, failure modes, and containment behavior of the prototypes were obtained from spin testing. Also, some of the program goals were approached and exceeded (Garrett multi-ring rotor, which attained an ultimate energy density of 79.4 Wh/kg and a stored energy of 1.23 kWh). In addition, improved understanding of composite rotor design, structural behavior, material responses, and fabrication processing was obtained from prolonged association with the variety of materials, constructions, and design features embodied in the prototype rotors. Spin testing permitted evaluation of the effectiveness of intricate design features to obtain high storage performance (for example, rotors developed by the Garrett and Brobeck organizations). Tests also revealed surprisingly high performance in exceedingly simple design such as the constant thickness laminated disk.

Since it was not possible to continue the development of all the rotor designs, an evaluation/selection process was conducted to identify the most promising concepts for further development and testing. The designs selected were the Garrett multi-ring rim type rotor and the General Electric ring/disk hybrid rotor. Ten prototypes of each of these designs were fabricated and several were spin tested for ultimate and cyclic endurance in a laboratory environment. An AVCO design was also developed further.

In addition to the rotor developments, two parallel studies were initially performed to provide a design basis for composite rotor containment (Refs. 3-4). These studies included an assessment of available containment technology for metallic and composite rotors, examination of composite rotor burst test data, and definition of containment housing design concepts. The methodology and design concept produced by General Electric was subsequently selected for further development. Experimental containment housings for the Garrett and General Electric flywheels were fabricated and one containment test involving a complete burst of a General Electric rotor was

performed. This test was the first of its kind (i.e., a high performance burst within a housing of pracitcal proportions) and revealed important realities of composite rotor containment processes.

This paper describes recent developments of the General Electric hybrid rotor design and discusses its relation to flywheel designs that are especially suitable for spacecraft applications. It also projects potential performance gains that can be achieved in such rotor designs by applying latest developments in materials, processing, and design methodology. Indications are that substantial improvements can be obtained.

Merit indices of composite flywheel performance include the following:

$$\text{Weight Energy - Density, } E_W, = \frac{\text{Stored Energy}}{\text{Total Rotor Weight}}$$

$$\text{Volume Energy - Density, } E_V, = \frac{\text{Stored Energy}}{\text{Rotor Swept Volume}}$$

$$\text{Cost Energy - Density, } E_C, = \frac{\text{Stored Energy}}{\text{Rotor Cost}}$$

These indices may be related to an ultimate storage capacity based on short-term failure and an operational capacity based on cyclic life. Similar indices may, of course, also be defined on a system level by referring to the weight, enclosed volume, and cost of the entire energy storage system.

Another set of indices considers only the rotors and containment housing and is of particular value in designing an optimum flywheel system. This is because the various rotor designs under consideration may have widely different containment requirements. A high performance rotor design might, for instance, have a highly destructive failure mode, thereby requiring relatively heavy containment. Because of this, its combined rotor and containment energy density might be lower than that of a lower performance rotor which has a relatively benign mode of failure.

In contrast to metallic (isotropic) flywheels, whose weight energy-density can be exprssed as

$$E_W = k \left(\frac{\sigma}{\rho} \right)$$

where k is the shape factor, σ the ultimate or operational strength, and ρ the mass density, the definition of a performance index is more complex for composite rotors. Such materials have distinctive and complex behaviors because of anisotropy and heterogeneity. The orthotropy in elastic moduli can introduce a strong coupling between geometry and material properties, the thin ring perhaps being an exception. Also, fiber composites have low strengths corresponding to failure modes that are controlled by matrix properties, and time-dependent properties can differ significantly from the static values usually quoted.

What is generally required for composite rotor designs is an accurate stress analysis of its component members and the identification of limiting failure modes. Each failure mode can be expressed in terms of a corresponding rotor peripheral speed.

Hence a set of limitng speeds can be defined for a given design, and from the lowest of these, minimum performance indications for the appropriate use conditions are determined.

DESIGN FEATURES OF THE HYBRID ROTOR

The hybrid rotor shown in Figure 1 is basically a solid, constant thickness disk configuration that consists of three parts: a central laminated disk, a filament-wound outer ring, and a small metallic hub that is attached to the disk. In the usual form of the design, the laminate is a quasi-isotropic layup of unidirectional plies of glass/epoxy prepreg material cured in a press. The fiber volume and void content have typically been 50 to 55 percent and 2 percent, respectively. The ring is usually constructed of high-strength type graphite/epoxy material with a fiber volume and void content of 60 percent and 1 to 25 percent, respectively.

The ring is fitted to the disk by means of a simple interference fit. Radial interferences of .001 to .002 in./in. of outside ring radius have been employed, with values in the lower range in more recent designs. The interference fit is accomplished by cooling the disk and ring. In the cooling process the disk diameter contracts while the graphite/epoxy ring remains dimensionally inert, thereby permitting the ring to be slipped over the disk. When the interference fit is in the vicinity of .002 in./in. mechanical pressing is required in addition to thermal action.

Stresses in the hybrid rotor are governed by the elastic properties of the disk and ring, the interference fit value, and the parameter β which is the ratio of the inner and outer radii of the ring. In previous prototype rotors, β values have ranged from about .73 to .82.

The ring serves the following functions: (1) it operates at high energy density, (2) the ring/disk interface pressure acts to reduce the disk tensile stresses slightly and also to reduce radial tensile stresses in the ring; (3) it prevents fraying and other edge effect problems of the disk, (4) it greatly improves the fatigue and creep performance of the disk because of the excellent fatigue and creep properties of graphite/epoxy and (5) it can alter the flywheel failure mode from disk rupture to a less severe ring burst mode.

A small aluminum hub/quill adapter is bonded elastomerically to the disk. The bond accommodates the large differential radial growth that occurs between the disk and hub adapter during rotation. It also provides damping, but this is probably a disadvantage because internal damping is known to have an adverse effect on dynamic stability.

In 1982, 14 hybrid rotors were produced by General Electric for LLNL for ultimate speed and cyclic endurance spin testing. Except for certain details the rotors were nominally identical in size and design energy storage capacity. Their properties are shown in Table 1. The storage capacities were nominally .5 kWh (ultimate) and .25 kWh at maximum operational speed. The differences among these rotors were due to the resin used for the matrix of the outer ring. The basic design (Type A) employed Epon 826 epoxy which had been used in previous hybrid rotors. Ten Type A rotors were produced. Types B and C used a high temperature epoxy (Ciba-Geigy CY-179) and a flexible polyurethane respectively. Two each of Types B and C were produced.

Table 1. Properties of General Electric Hybrid and Simple-Disk Flywheels

Parameter	Hybrid	Simple Disk
Rotor OD, in.	16.00	15.86
Ring ID, in.	12.80	-
Ring Thickness, in.	1.74	-
Disk Thickness, in.	1.67	1.70
Rotor Weight, lb.	22.33	23.44
Rotor Weight, less Hub, lb.	21.22	22.33
Polar Moment of Inertia, lb-in.-sec^2	1.69	1.82
Swept Volume, ft^3	.202	.194

Also, simple laminated disk rotors were produced (Table 1), mainly to obtain basic spin test data about failure stress levels and failure modes of the laminate. The rings and laminates were fabricated by the Lord Corp. and 3M Co., respectively.

PERFORMANCE TESTS

Two ultirate speed tests and one cyclic spin test were performed on hybrid rotors (Nos. H8/GE-F and H6/GE-J) and one ultimate speed and one cyclic test was conducted on a simple laminated disk rotor (D2/GE-D). The test conditions and performances are listed in Table 2. Rotors H8 and D2 were the only units that were subjected to the cyclic testing and both rotors successfully endured the required 10,000 spin cycles. Each cycle consisted of spinning between energy levels of 217 and 54.2 Wh over a 6.5 minute period for the hybrid rotor and between 190 and 47.4 Wh over an 8.0 minute period for the simple disk rotor. After completion of the cyclic tests, these same rotors were tested for ultimate burst capacity. Rotor H8 burst at an energy level of 650 Wh and energy density of 68.0 Wh/kg. The peripheral speed at failure was 1,010 m/sec, believed to be the highest value ever attained in a flywheel. Rotor D2 burst at an energy level of 529 Wh and energy density of 52.1 Wh/kg. The basis for computing the energy level and energy density is as defined in Ref. 4.

The only other hybrid rotor that was brought to its ultimate speed was rotor H6 which burst at an energy level of 648 wh and energy density of 67.0 Wh/kg. This result was most interesting for several reasons, first because rotor H6 had not been previously tested and yet its burst performance very nearly duplicated that of rotor H8 which had been cycled 10,000 times. Also, the failure mode of both rotors was the same (i.e., circumferential burst of the outer ring). This set of data provides

Table 2. Cyclic and Ultimate Spin Test Results
for General Electric Hybrid and Simple Disk Flywheels

	Rotor Number (Type)		
	H8/GE-F (Hybrid)	H6-GE-J (Hybrid)	D2/GE-D (Simple Disk)
Cyclic Test			
No. of Cycles	10,000	-	10,000
Cycle Duration, minutes	6.5	-	8.0
Speed: rpm, max. (min.)	27,330(13,660)	-	24,600(12,300)
m/s, max. (min.)	583(292)	-	519(260)
Energy, Wh, max. (min.)	217(54.2)	-	190(47.4)
Weight, lb.(1)	21.27	21.32	22.38
E_W, Wh/kg	22.5	-	18.7
E_V, kWh/m^3	37.9	-	34.6
Ultimate Test			
Ult. Speed, rpm (m/s)	47,058(1,010)	46,602(992)	40,638(867)
Energy, Wh	656	648	529
E_W(2), Wh/kg	68.0	67.0	52.1
E_V(2), kWh/m^3	115	113	94

(1) Not including 1.11 lb Hub Arbor.

(2) Based on Dimensions at Ultimate Speed.

the only existing indication of the effect of significant spin-cycling on the ultimate performance of a composite flywheel. At least for these two test points, the performance appears to be rather unaffected by the cycling imposed.

Based on the high ultimate energy density exhibited in these tests the operational level of a hybrid rotor of the design represented here would appear to be about 40 Wh/kg. The operational level imposed in the cyclic test of rotor H8 reflected the lower ultimate performance that had been expected, as well as a degree of caution in approaching this unprecedented test. More will be said later about the significance of these test results.

Attempts to reach ultimate burst conditions were made unsuccessfully with three other duplicate hybrid rotors. The tests, however, were significant because they manifested the ruggedness of the rotor construction, especially the graphite/epoxy ring component, and contributed to a better understanding of the loose-rotor containment process. In each case, the rotors separated from the drive shaft due to a whirl resonance condition that developed prior to attainment of a burst speed condition. The speeds at which separation occurred ranged between 35,820 and 40,910 rpm or 769 and 878 m/sec. Subsequent to separation, the rotors spun within the containment ring, finally coming to rest within one minute. Except for some graphite/epoxy which had been smoothly ground away during the spin-down process, the rotors were recovered in an intact condition.

FAILURE MODES OF HYBRID ROTORS

A plane stress analysis considering a quasi-isotropic disk and orthotropic outer ring and a uniform interface pressure between the two is used to calculate the stresses and deformations of the hybrid rotor system. The analysis (Refs. 6-7) provides an accurate and convenient means of optimizing the design of hybrid rotors. This facility is due basically to the constructional simplicity and axial symmetry of the rotor. The result is that for given component materials, the rotor stresses, displacements, and interface pressure are expressable in terms of three design parameters, namely, the ring radius ratio, $\beta = a/b$, unit radial interference $\bar{\delta} = \delta/b$, and rotor peripheral speed, V. Here a and b are respectively the inside and outside radii of the ring and δ the radial interference. Hence the maximum allowable speeds V_i can be determined with respect to each of the governing failure modes of the hybrid system for any set of values β and $\bar{\delta}$. These modes are as defined in Table 3, in which the starred quantities are the maximum allowable design stresses for ultimate or fatigue failure conditions. Symbols in the table are defined as follows: CRF, circumferential ring, PRF, radial (transverse) ring, and DF, disk failure; S, ring/disk separation; B, bearing failure; $\sigma_{\theta R}$, circumferential ring, σ_{rR}, radial ring, and σ_D, disk center stress or strength; σ_B, bearing strength at ring/disk interface; and P, interface pressure.

A composite plot of V_i vs β for the i failure modes clearly exhibits the allowable operational regime for rotor systems having a given value of $\bar{\delta}$. The rotor energy/weight ratio E_{w_i} (energy density), expressable in terms of β and V_i, is more usually plotted instead of V_i. The author has referred to such a representation as a Nimmer plot. Data for constructing Nimmer plots are obtained by means of a computer program which calculates the energy densities E_{W_i} for all failure modes and the interface pressure at rest, P_o, for a specified range of β. It also calculates, if applicable, the value of β above which the interface pressure increases with increasing rotor speed. In this particular β range, the ring will remain in contact with the disk even if the initial interference is zero.

Table 3. Definition of Governing Failure Modes of Hybrid Rotors

Failure Mode	Symbol	Condition for $V = V_i$
Circumferential Ring Failure	CRF	$\sigma_{\theta R} = \sigma_{\theta R}^*$
Radial Ring Failure	RRF	$\sigma_{rR} = \sigma_{rR}^*$
Disk Failure	DF	$\sigma_D = \sigma_D^*$
Ring/Disk Separation	S	$P = 0$
Interface Bearing Failure	B	$P = \sigma_{BR}^*$ or $= \sigma_{BD}^*$

A meaningful interpretation of a Nimmer plot requires careful consideration of ring/disk loading interactions in the light of uncertainties in governing material property values. These uncertainties are due to (1) limited available standard specimen data, (2) fabrication process dependency, (3) size effects, and (4) variation of certain properties with load and time.

A Nimmer plot that was used for the initial design selection of the present hybrid rotors (Types A and B) is shown in Figure 2. It is based on moderately heavy interference fit of .002 in./in. and the materials data of Table 4. The plot shows energy density (Wh/lb) versus radius ratio β for the various governing failure modes and serves to identify the optimum range of β. The present hybrid rotors were designed with $\beta = .8$; therefore, the limiting failure mode indicated is CRF for ultimate failure (solid curve) and either CRF or DF for the 10^5 cycle operational conditions (dashed curves). In most cases the failure modes for high β values (thin rings) is DF or CRF while for low β values (thick rings) it is RRF or S (the latter for light interference fits).

ANALYSIS OF SPIN TEST DATA

The design data of Table 4 were compiled from previous hybrid rotor developments (Refs. 6, 7 and 8), available rotor spin test (Refs. 8-9), specimen test data (Refs. 6-8, 10-13), and laminate analysis (Ref. 15). As more spin test data became available for hybrid and simple laminated disk rotors, they were studied by means of the rotor structural analysis to refine the assessment of material strength values. In doing this the older spin test data were reexamined to reduce all conclusions regarding strength to a reasonably consistent basis. This study, described in Ref. 16, led to several important conclusions. First, the elastic modulus of the laminated disk becomes degraded due to the development of distributed microcracks in the laminate resin as the stresses in the disk exceed threshold levels. In hybrid rotors, the principal effects of this are to reduce the stresses in the disk and increase the

Table 4. Properties of Prototype Rotor Materials: Disk (S-2 Glass/SP250 Epoxy); Ring (T-300 Graphite/Epon 826 Epoxy)

Item	Disk				Ring					
	E_D, msi*	σ_D, ksi	ρ_D, lb/in.^{3}	ν_D	$E_{\theta R}$, msi*	E_{rR}, msi*	$\sigma_{\theta R}$, ksi	σ_{rR}, ksi	ρ_R, lb/in.^{3}	ν_R
Ultimate	3.3	60	.066	.3	18.8	1.40	170	2.0-3.5	.0531	.3
10^5 Cycles	2.55	25	.066	.3	18.8	1.40	117	1.2	.0531	.3

*1 msi = 1,000,000 lb/in.^{2}

circumferential stress ($\sigma_{\theta R}$) and reduce the radial tensile stress (σ_{rR}) in the ring. Second, as a direct consequence of this, when the failure mode is CRF, the strength $\sigma_{\theta R}$ is greater than those values, based on the initial disk modulus, and when the mode is RRF, the tensile strength σ_{rR} is smaller.

The revised estimates of design strength values were inferred from the calculated stress results that correspond to observed failure modes of tested rotors. In some cases, a lower bound estimate was obtained for a particular failure mode that was not the actual mode of failure in the test. The stress results are summarized in Table 5, which embodies most of the available spin tests of hybrid and simple disk rotors having 0, 90, +45, -45° laminate ply construction. The stresses listed do not include residual stress. All the hybrid rotors except the second set of tests 80-3 and 80-4 have two listings of data, the first corresponding to the initial disk elastic modulus and the second to the reduced modulus. The most important effects of the reduced disk modulus pertain to the outer ring.

The radial tensile stress σ_{rR} is addressed first. Only in Tests No. 80-3 and 4 did the RRF mode actually occur. The average calculated stress for these tests at the location at which failure was observed to occur is 1.71 ksi for the reduced modulus and 2.66 ksi for the initial modulus. Adding to these an estimated .5 ksi due to fabrication-induced residual stress we obtain values of 2.2 and 3.2 ksi for the radial tensile strength. The lower value, especially as it is associated with the reduced disk modulus, is assumed to be the indicated σ_{rR} strength. In the H8 and H6 tests, in which RRF did not occur, the maximum calculated radial stress corresponding to the reduced modulus is 1.46 ksi and the calculated residual stress is .482 ksi (Ref. 16). Hence, the total σ_{rR} = 1.94 ksi, which compared to the above strength value (2.2 ksi) is consistent with a non-radial failure condition. If, on the other hand, the calculated values of σ_{rR} for Tests No. 80-3 and 80-4 corresponding to the initial modulus were used as a basis for estimating the σ_{rR} strength, this would yield an average value of 2.66 + .5 = 3.1 ksi. But the average calculated σ_{rR} (based on the initial disk modulus and including residual stress) for the H8 and H6 tests is 3.5 ksi, or greater than the indicated strength. This would not be consistent with the fact that RRF did not occur in these latter two tests. Hence, the four tests taken together support the existence of a reduced disk modulus and an estimated σ_{rR} strength of about 2.2 ksi. In Ref. 16, transverse tensile test data obtained on specimens cut from rings identical to those used in the 80-3 and 4 tests yielded an average strength of 3.23 ksi. A

Table 5. Rotor Stresses Analytically Deduced from Spin Tests of Hybrid and Simple Disk Flywheels

Test No.	Type	β	δ	Failure Mode	E_D	$\sigma_{\theta R}$	σ_{rR}	σ_{D_o}
80-3	Hybrid	.75	.002	RRF	3.0 2.28	134 144	1.9 1.1	33
80-4		.72	.002	RRF	3.0 2.17	149 163	3.5 2.4	38
80-3		.75	.002	NF	3.0	171	-	-
80-4		.72	.002	NF	3.0	180	-	-
80-8		.82	.002	CRF	3.1 2.15	156 179 200	.7 3.4	47 71
H-8		.80	.00111	CRF	3.3 2.2	239 222	1.6 2.7	64 70
H-6	Hybrid	.80	.00168	CRF	3.3 2.2	239	1.3	61
80-2	Simple Disk	-	-	DF	-		-	106
D1		-	-	NF	-		-	75
D2		-	-	DF	-		-	81
D5	Simple Disk	-	-	NF	-		-	81

'size effect' factor accounting for the probability of internal flaws was applied to the raw data to yield an estimated strength of 1.6 ksi. Hence, the deduced strength 2.2 ksi (above) might indicate that the strength of the material in the ring state is greater than in the test coupon condition, with the computed 'size effect' of Ref. 6, maintained. Such a conclusion was reached in Ref. 15, also for the case of longitudinal (circumferential) strength, i.e., $\sigma_{\theta R}$ is greater in the ring than indicated by specimen tests.

Next the circumferential stress $\sigma_{\theta R}$ is addressed. In the 80-3 and 80-4 tests, after the occurrence of RRF, the rotor speeds were subsequently increased until whirl-induced vibrations caused the rotor to separate from the drive shaft. During this interval of time, the graphite/epoxy ring in each case was divided into two ring portions mutually detached along the radial positions at which RRF occurred. In this condition interface pressure between the ring portions would not exist. Hence, the disk elastic modulus would not have any effect on the stresses in the outer ring portion. The second listing of $\sigma_{\theta R}$ for these tests represents the maximum value in the outer ring portion at the highest speed attained (not including the residual stress, estimated to be about 4 ksi). Therefore, the $\sigma_{\theta R}$ strength must have been greater than the listed value plus the residual stress, or greater than 175 (10-3) and 184 (80-4) ksi.

In Test No. 80-8, the ring failed in CRF. The calculated maximum value of $\sigma_{\theta R}$ corresponding to the reduced modulus and including a residual stress of 7 ksi is 186 ksi. The rotor is suspected to have had an interference fit greater than the identified value of .002 in./in. because it required a heavy mechanical force in addition to thermal contraction of the disk to assemble the two components. Assembly with an interference fit of .0022 in./in. can be accomplished solely by thermal action. Accounting for this, it is estimated the ring manifested a strength of 190-195 ksi.

The circumferential ring strengths exhibited by these hybrid rotors produced in a previous program (Refs. 6-8) are substantially greater than the design value of 170 ksi used for the present rotors (Table 4). The tests of the present rotors, H8 and H6, also support these indications, except to a considerably greater extent. The $\sigma_{\theta R}$ values corresponding to the reduced disk modulus for these rotors are identical, equal to 248 ksi (including a residual stress of 9 ksi determined in Ref. 16). The equality of the two values of $\sigma_{\theta R}$ is in fact remarkable, considering the differences in δ, densities of disk and ring materials, and failure speeds. These values were carefully determined and were used in the calculation of $\sigma_{\theta R}$. It is noted that the calculated values of $\sigma_{\theta R}$ based on the initial disk modulus are not equal, and also that the values corresponding to the initial modulus are quite high (e.g., 222 + 9 = 231 ksi for rotor H6). Hence, these unexpectedly high but plausible values of $\sigma_{\theta R}$ are considered to be reasonably well established.

Another important point that can be made about the pair of tests is that rotor H8 is known to have possessed extensive resin microcracking prior to the performance of the ultimate speed test. This had developed during the 10,000 cycle spin test which preceded it. Visual examination of the lateral surfaces as well as ultrasonic C-scans of rotors D2 and H8 that were made after completion of the cyclic testing revealed this fact. Hence, ample evidence exists to support the assertion that a reduced modulus was indeed present in the disk during the subsequent burst test. The only question remaining is the exact value of it. However, any reduction in modulus whatever would result in an indicated $\sigma_{\theta R}$ strength greater than 209 ksi. Also, the almost identical performance of rotor H6 which had not been tested in any way prior to its burst test would suggest that resin microcracking is a short-term phenomenon in a glass/epoxy laminate of the type represented here (i.e., it develops simultaneously with the onset of sufficiently high stresses).

The recently performed spin tests of simple laminated disk rotors (D1, D2, and D5) listed in Table 5 support the indication of the earlier test (80-2) that the biaxial strength of quasi-isotropic S-glass/epoxy laminates (0, 90, +45, -45°) is considerably higher than indicated by specimen tests (Table 4). The recent tests were specifically intended to show whether the high strength exhibited in Test No. 80-2 could be realized. The question was not answered because attempts to reach short-term burst were thwarted by separation failure of the rotor (D1 and D5) from the drive shaft following the development of a whirl resonance vibration. However, all the simple disk rotors exhibited strengths of at least 75-81 ksi at the maximum attained speed. This compares to the 60 ksi value used for the recent disk designs. The result of the D2 test, however, is very significant. The rotor successfully completed the 10,000 cycle test prior to undergoing the ultimate speed test that resulted in the burst. The peak center stress during the cyclic test was 30 ksi. Since the calculated center stress at burst was 81 ksi, it is probable that the short-term ultimate strength is considerably higher than this. In itself the D2 test indicates that the 10^4 cycle fatigue strength is probably considerably greater than 30 ksi.

Revised tentative design data based on Table 4 and Ref. 16 are shown in Table 6 for hybrid rotors of the type discussed herein. The 10^5 cycle fatigue values for $\sigma_{\theta R}$ and σ_{D0} are multiplied by knock-down factors of .68 and .42 used in the recently tested rotor designs. The ultimate value of E_D reflects the conclusion stated above that the reduction in disk modulus due to resin microcracking is a short-term phenomenon.

Table 6. Revised Tentative Properties of Hybrid Rotor Materials: Disk (S-2 Glass/SP250 Epoxy); Ring (T-300 Graphite/Epon 826 Epoxy); Poisson's Ratio = .3

Item	Disk			Ring				
	E_D, msi*	σ_D, ksi	ρ_D, lb/in.^{3}	$E_{\theta R}$, msi*	E_{rR}, msi*	$\sigma_{\theta R}$, ksi	σ_{rR}, ksi	ρ_R, lb/in.^{3}
Ultimate	2.2	>81	.067	18.8	1.4	248	2.2	.0535
10^5 Cycles	2.55	>34	.067	18.8	1.4	168	1.2	.0535

*1 msi = 1,000,000 lb/in.^{2}

A Nimmer plot of designs based on the properties of Table 6 and an interference fit of .00168 in./in. is shown in Figure 3. The solid and dashed lines indicate the governing failure envelopes for ultimate and maximum (10^5 cyclic life) operational speeds respectively. An optimum ultimate energy density of 30.3 Wh/lb (66.8 Wh/kg) occurs at β = .78. Designs with higher β values are governed by CRF and lower β values by RRF. The operational speed failure envelope is governed by DF on the left and RRF on the right and represents two different values of disk strength (10^5 cyclic life) of 34 ksi (lower) and 42 ksi (upper). These values correspond to ultimate strengths of 81 ksi, discussed previously, and 100 ksi, a capability demonstrated in Test No. 80-2 (Table 5). The optimum operational energy densities for these values of σ_D are respectively 17.5 Wh/lb (45.2 Wh/kg) at β = .78. The design of rotor H6 is positioned on the plot at β = .8.

In addition to demonstrating high overall performance, the tests of rotors H8 and H6 yielded important data about the ultimate and cyclic energy storage capability of the graphite/epoxy ring component. These are summarized in Table 7, in which W_R and I_R are the weight and polar moment of inertia of the ring. The outer ring of rotor H8, which had been cycled 10,000 times between maximum and minimum energy density levels of 38.5 and 9.6 Wh/kg, later attained an ultimate energy density of 116 Wh/kg. Similarly, the previously untested ring of rotor H6 attained an ultimate value of 114 Wh/kg. Such high performance levels demonstrate the potential of flywheels that are constructed of similar filament-wound rings.

Table 7. Energy Storage Performance of the Ring Component of Rotors H8 and H6 as Obtained from Spin Tests

Rotor No.	Parameter					
			Ultimate		10^5 Cycles	
	W_R, lb	I_R, lb-in.-sec^2	E, Wh	E_W, Wh/kg	E, Wh	E_W, Wh/kg
H8	6.79	.922	358	116	119	38.5
H6	6.73	.913	348	114	-	-

TOWARD HIGH PERFORMANCE SPACE FLYWHEELS

It is desirable to employ designs that utilize radially thicker rings of such materials in order to obtain still higher energy density and an internal diameter that is more suitable for interfacing with other system components. Unfortunately, such designs are precluded due to the low radial tensile strength of present filament-wound materials. This characteristic is apparent in Figure 3 wherein the RRF mode governs designs having $\beta < .77$, or thickness $t > .23\ b$, where b is the ring outside radius. Beyond this limit thicker ring designs are accompanied by steadily lower energy densities. Measures to remedy this limitation exist, however, at least theoretically. Two approaches have been discussed, namely, the multi-ring design (Refs. 17-18) and the flexible-matrix design (Refs. 19-20).

The multi-ring approach employs concentric rings that are assembled with suitable interference fits. The radial pressures thereby produced at the interfaces between rings set up initial radial compression stresses in the ring components. Under rotational conditions, these pre-stresses act to decrease the radial tensile stresses. Beneficial effects on the circumferential stresses can also be obtained by this method.

The other approach utilizes a flexible instead of rigid matrix in the ring material. Such construction results in a greatly reduced radial modulus of elasticity without affecting the circumferential modulus. Analysis shows that by proper construction, such a material can provide a radial strain capacity high enough to avoid radial failure even in very thick rings.

Another contribution to high performance rotor design is the utilization of new high strength (graphite, aramid) fibers that are now available. The graphite fibers have at least 50 percent greater strength than the type used in the present GE hybrid flywheels. This promises to yield a similar increase in energy density.

Up to the present time, two GE hybrid rotors incorporating flexible-matrix graphite fiber rings ($\beta = .8$) have been fabricated. To the author's knowledge, no multi-ring rotors specifically utilizing graphite/epoxy rings have been produced.

Preliminary studies at General Electric have identified two generic flywheel designs that incorporate a thick, flexible-matrix ring, namely the concentric and tandem arrangements. They differ in the manner in which the motor/generator is mounted to the flywheel

In the concentric arrangement the motor/generator is mounted and supported within the bore of the rotor ring, as shown in Figure 4. The advantages of this design are overall compactness and efficient placement of high energy density material within the assigned envelope. This is due to the absence of a central hub component. Disadvantages include limited design flexibility to incorporate other flywheel components and greater expected difficulty of cooling the rotating parts of the motor/generator.

Preliminary design estimates of rotors based on the concentric type ($\beta = .5$) are listed in Table 8 for useful energy storage capacities of 2.5 and 5 kWh (75 percent depth of discharge (DOD). The estimates are based on the high strain graphite fiber. The useful energy density is 79 Wh/kg and the energy densities at 100 percent operational and ultimate speeds are 105 and 155 Wh/kg respectively. These values are based on the rotor weight alone.

Table 8. Design Concept Estimates for Space Station Size Flywheels (Concentric Type)

Parameter	Operational Energy at 75% DOD	
	2.5 kWh	5.0 kWh
OD, in.	20.8	26.0
ID, in.	10.3	13.0
h, in.	5.2	6.5
W, lb	70	139
J, lb-in.-sec^2	12.0	38.2
100% Op. Speed, RPM	40,100	31,800
E (75% DOD)	2.5	5.0
Useful Energy Density, Wh/kg (Rotor alone)	79	79

The tandem arrangement utilizes a relatively small diameter hub that is supported by means of a shrink fit within the rotor bore, as shown in Figure 5. Calculations show that it is feasible to employ a low weight metallic hub, a feature that greatly facilitates mounting of other components to the flywheel rotor. The tandem arrangement offers very significant advantages over the concentric type, namely enhanced design flexibility because it decouples the radial growth characteristics of the rotor bore and the motor/generator and does not restrict the selection of the latter's length/diameter ratio. In addition, cooling of the rotating portion of the motor/generator is facilitated due to its direct exposure to cooling sources. It also

permits greater bearing spans. The energy density that is estimated for the tandem design is somewhat less than that of the concentric type because of the presence of the hub. Performance estimates are listed in Table 9 for β ratios of .2 and .4. The respective useful energy densities being 76 and 70 Wh/kg.

Table 9. Calculated Energy Densities of Tandem Type Thick Ring Flywheel Rotors Constructed of High-Strain Graphite/Flexible Matrix Material

β	Rotor Energy Density (Wh/kg)		
	Ultimate	10^5 Cycles (100% DOD)	10^5 Cycles (75% DOD)
.2	146	101	76
.4	134	93	70

CONTAINMENT DESIGN APPROACH

Such high rotor performance levels indicate the growth potential offered by flywheels for space power applications. Recent experience has begun to show, however, that the weight penalties to provide for safe containment of a high energy rotor burst are likely to be prohibitive. It is important, therefore, to seek an early resolution to the issue of containment. Fortunately design and spin test experience, especially with ring/disk hybrid rotors, suggests that successful resolution of the issue may be obtained through proper rotor design.

The approach to this is to design rotors whose failure is accompanied by either zero or minor release of fragmentation. Such failure characteristics are theoretically obtainable in composite rotors by designing to a RRF mode or employing a flexible matrix in the ring construction. In the RRF mode, which is obtained with relatively thick, rigid-matrix rings, a circumferential crack is generated in the matrix between fibers. This does not significantly affect the circumferential strength of the ring but does disturb the rotor balance. The occurrence of RRF therefore produces a signal for initiating a safe shutdown of the rotor. There are at least two well documented instances in which RRF occurred in hybrid rotors (Tests No. 80-3 and -4 discussed previously). In each case the rotors were spun to considerably higher speeds after the occurrence of RRF. Subsequently they exhibited further ruggedness when they spun down to rest against the test chamber following separation from their drive shafts. Hence, there is good support for considering the RRF mode a practical basis for non-burst rotor design.

Flexible matrix rotor design has a potential for minor containment requirements because failure (CRF) should initiate very near the outside periphery of the rotor. In such an event, breaks in fibers would occur there, resulting in a disturbance of the rotor balance. This would provide a signal to shut down the unit. In the process it is quite possible that some minor fragmentation would be released from the outer surface of the rotor, thus necessitating use of a light-weight shield under certain

circumstances. The failure process, however, is considered to be self-arresting since the region radially inboard of the failure zone is at a lower stress level. This situation contrasts with the circumferential failure process involved in a rigid-matrix rotor ring. There, CRF occurs at the inside radius of the ring and material in the failed zone exerts its full centrifugal load on outer portions of the ring. Once this happens, the process can progress until the entire ring fails circumferentially. No test experience exists, however, for rotors utilizing flexib matrix rings.

Extensive testing is required to establish the practicality of high performanc flywheel rotors whose failure is governed by zero or minor fragment-release modes. The technical grounds for expecting success are quite sound and the benefits of minimizing or eliminating the containment requirement manyfold. If this can be achieved, a combined useful energy density of about 40 Wh/kg at 75 percent DOD (including motor-generator, bearings, and electronics) could result for the advanced space flywheel power system.

CONCLUSIONS

1. Of the two General Electric composite hybrid rotors that have been tested to ultimate speed, burst energy densities (and stored energies) of 67 Wh/kg (648 Wh) and 68 Wh/kg (656 Wh) have been obtained. Based on this, the 10^5 cycle operational energy density at 100 percent DOD is projected to be 40 Wh/kg.

2. One of the above flywheels (656 Wh, H8) completed 10,000 spin cycles, each involving a 6.5 minute duration and maximum and minimum stored energies of 217 an 54 Wh (75 percent DOD), prior to the ultimate speed test.

3. The pair of ultimate speed tests indicated no degradation in ultimate performan due to the 10^4 cycles.

4. The graphite/epoxy rings of the two rotors demonstrated ultimate energy densiti of 114 and 116 Wh/kg. One of these (see conclusion no. 2) successfully complet 10,000 spin cycles at a maximum energy density of 38 Wh/kg (100 percent DOD) prior to the ultimate speed test. These data show the high potential of filame wound graphite/epoxy ring components for use in flywheel space power systems.

5. Analysis of the high ultimate energy performance of hybrid rotors H6 and H8 ha led to the conclusion that the circumferential strength of the T-300 graphite/ Epon 826 epoxy composite rings used in the rotors is much greater than suggeste by standard materials tests.

6. The low radial (transverse) tensile strength of filament-wound graphite/epoxy material limits the radial thickness to about 20 percent of the outside diamete This can be extended somewhat by employing a radial compression pre-stress, as from a radial interference fit.

7. Large radial thicknesses are possible, however, when a flexible matrix is substituted for the standard rigid epoxy matrix of the ring. With this technique high energy densities are theoretically indicated.

8. Large, possibly prohibitive, penalties are associated with a requirement to contain a high energy composite rotor burst. A better approach is to design a rotor which is either fail-safe (no fragments released at failure) or releases a minor amount of fragmentation. Such failure characteristics are identified with particular rotor designs.

9. Utilizing a fail-safe rotor design and available 700 ksi graphite fibers in the ring component, advanced flywheels exhibiting operational energy densities as high as 105 Wh/kg (rotor alone and at 100 percent DOD) are indicated by design calculations.

REFERENCES

1. Notti, J.E., Cormack, A., III, and Schmill, W.C., "Integrated Power/Attitude Control System (IPACS) Study," Vol. I, NASA CR-2283, April 1974.

2. Notti, J.E., Cormack, A., III, and Schmill, W.C., "Integrated Power/Attitude Control System (IPACS) Study, Vol. II, NASA CR-2284, April 1974.

3. Coppa, A.P., "Energy Storage Flywheel Housing Design Concept Development", General Electric Company; LLNL, Report No. UCRL-15448, S/C 6624409, March 12, 1982.

4. Sapowith, A.D. and Handy, W.E., "Composite Flywheel Burst Containment", AVCO, Proceedings of the Mechanical, Magnetic, and Underground Energy Storage 1981 Annual Contractors' Review, Conf-810833, February, 1982.

5. Coppa, A.P. and Kulkarni, S.V., "Composite Flywheels: Status and Performance Assessment and Projections" Proceedings of the II European Symposium on Flywheel Energy Storage, G. Genta, Ed., Torino, Italy, May, 1983.

6. Nimmer, R.P., Torossian, K., and Wilkening, W.W., "Laminated Composite Disk Flywheel Development", General Electric Company Report No. SRD-81-051, Fourth Interim Report, Subcontract No. 2479309, January, 1981.

7. Nimmer, R.P., et.al., "Laminated Composite Disc Flywheel Development", General Electric Company Report No. SRD-79-016, January, 1979.

8. Nimmer, R.P., Torossian, K., and Hickey, J., "Laminated Composite Disk Flywheel Development", General Electric Company, Report No. SRD-80-091, 1980. (Also LLNL Report No. UCRL-15301, February 1980.)

9. Rabenhorst, D.W. and Wilkinson, W.O., "Prototype Flywheel Spin Testing Program", Johns Hopkins Applied Physics Laboratory; LLNL Report No. UCRL-15381, April, 1981.

10. Rotem, A. and Nelson, H.G., "Fatigue Behavior or Graphite-Epoxy Laminates at Elevated Temperatures", ASTM-STP-723, Fatigue of Fibrous Composite Materials, 1981.

11. Awerbuch, J. and Hahn, H.T., "Fatigue and Proof Testing of Unidirectional Graphite/Epoxy Composite", ASTM STP 636. Fatigue of Filamentary Composite Materials, 1977.

12. Davis, J.W. and Sundsrud, G.J., "Fatigue Data on a Variety of Non-Woven Glass Composites for Helicopter Rotor Blades", 34th Annual Technical Conference, 1979 Reinforced Plastics/Composites Institute, Society of the Plastis Industry, Inc., 1979.

13. Mandel, J.F., "Fatigue Behavior of Fiber-Resin Composites", MIT Research Report R81-2, April, 1981.

14. Kulkarni, S.V., Reifsnider, K.L., and Boyd, D.M., "Composite Flywheel Durability and Life Expectancy: Test Program," Proceedings of the Mechanical, Magnetic, and Underground Energy Storage 1981 Annual Contractors Review, U.S. Department of Energy CONF 810833, February 1982.

15. McLaughlin, P.V., Dasgupta, A. and Chun, Y.W., "Composite Failure Analysis for Flywheel Design Applications:, Villanova University; LLNL Report No. UCRL-15296, S/C 6448409, March, 1980.

16. Coppa, A.P., "Composite Ring - Disk Flywheel Design, Fabrication, and Testing", General Electric Company Document No. 83SDS4248, Final Report to Lawrence Livermore National Laboratory on Subcontract No. 6624409, Tasks 12-16, August, 1983.

17. Kirk, J.A., Studer, P.A., and Evans, H.E., "Mechanical Capacitor" NASA TN D-8185, November 1975.

18. Flanagan, R.C., Wong, J.M., and Munro, M.B., "Fibre Composite Rotor Selection and Design", 17th IECEC Proceedings, Vol. 4, pp. 1961-1966, August 1982.

19. Gupta, B.P. and Lewis, A.F., "Optimization of Hoop/Disk Composite Flywheel Rotor Designs", 1977 Flywheel Technology Symposium Proceedings, CONF-771053, pp. 111-118, October 1977.

20. Coppa, A.P., "Composite Hybrid Flywheel Rotor Development", Monthly Progress Report No. 6, LLNL Subcontract 6624409 Tasks 12-16, 28 February 1982.

NOMENCLATURE

a,b	inside and outside radius of ring; $a/b = \beta$
B	bearing failure
CRF	circumferential ring failure
DOD	depth of discharge
DF	disk failure
E	energy
E_C	cost energy minus density
E_D	modulus of elasticity of disk material
E_R	modulus of elasticity of ring material
E_{rR}	modulus of elasticity of ring material in radial direction
E_V	volume energy minus density
E_W	weight energy minus density
$E_{\theta R}$	modulus of elasticity of ring material in tangential direction
h	height
I_R	polar moment of inertia
J	inertia
k	shape factor
P	interface pressure
RRF	radial (transverse) ring failure
S	ring/disk separation
V	rotor peripheral speed
V_i	maximum allowable speed
W	weight
W_R	weight of ring
β	ratio of inner to outer disk radius
δ	radial interference
$\bar{\delta}$	unit radial interference; $\bar{\delta} = \delta/b$
ν_D	Poisson's ratio for disk material
ν_R	Poisson's ratio for ring material
ρ	mass density
ρ_D	density of disk material
ρ_R	density of ring material
σ	ultimate (operational) strength
σ_B	bearing strength
σ_D	strength of disk material

σ_{DO}	stress at center of disk
σ_{rR}	strength of ring material in radial direction
$\sigma_{\theta R}$	strength of ring material in tangential direction

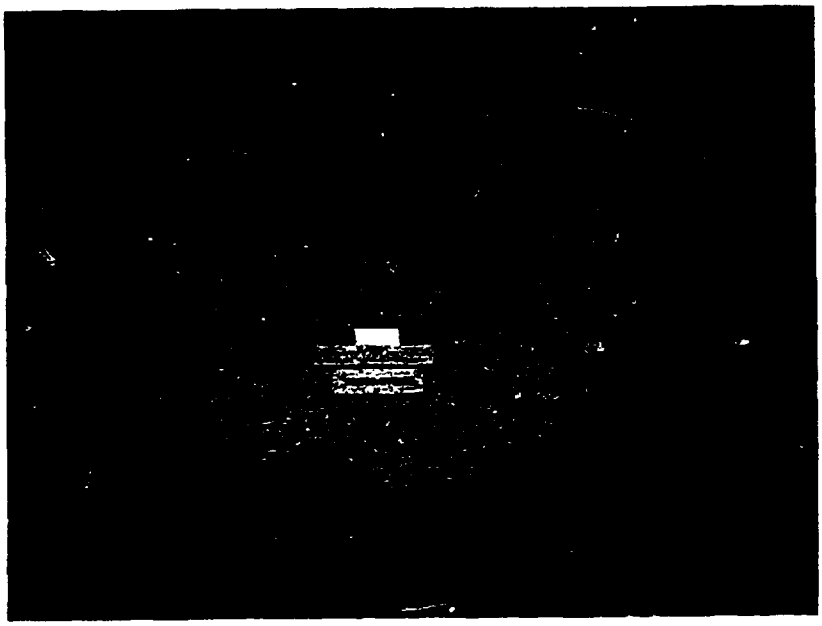

Figure 1.- Hybrid rotor no. H8-3M6-R14 after successful completion of 10,000-cycle 1083-hour spin test.

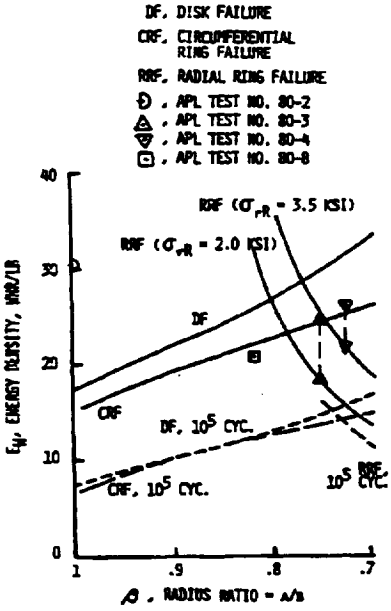

Figure 2.- Hybrid rotor energy density vs radius ratio for governing failure modes ($\bar{\delta}$ = .002).

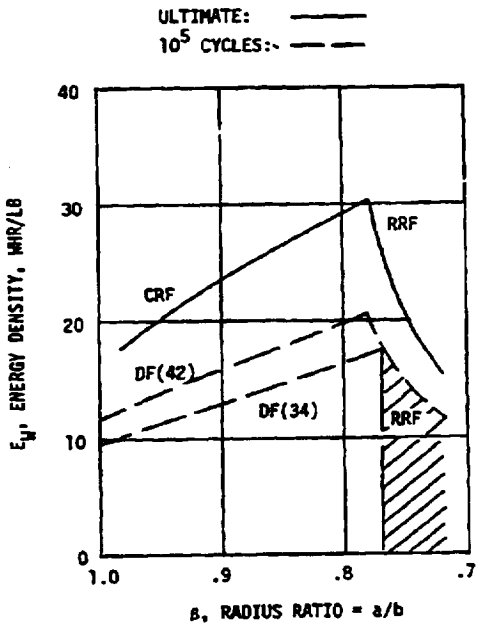

Figure 3.- Energy density vs radius ratio for for improved hybrid rotor designs based on revised properties of Table 6.

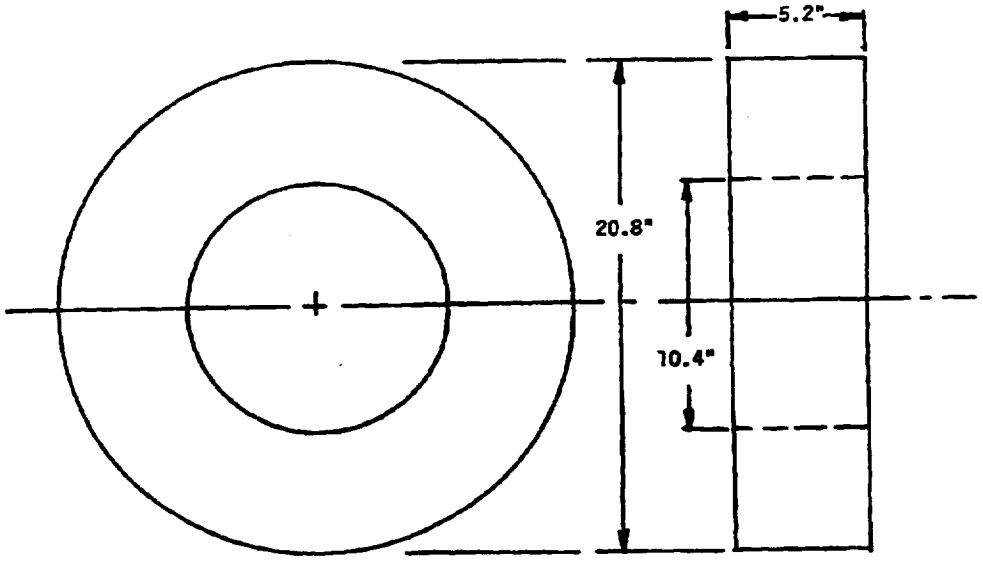

Figure 4.- Annular flywheel concept, concentric type (2.5 kWh). Rotor components mounted in bore.

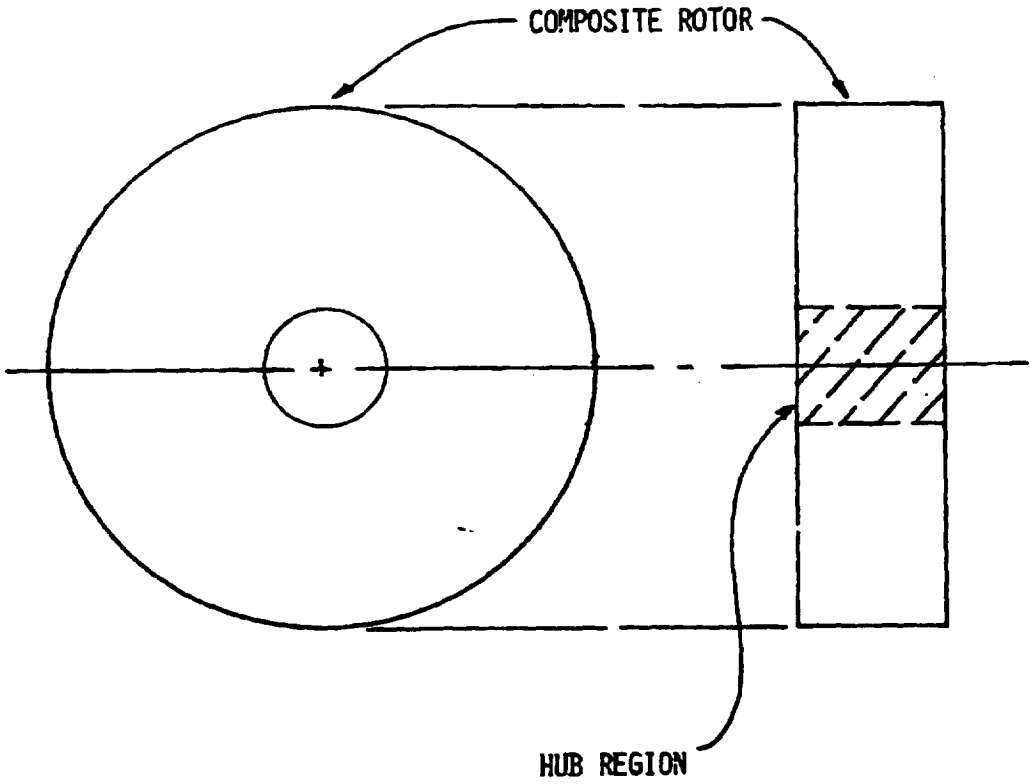

Figure 5.- Annular flywheel concept, tandem type, suitable for side mounting of rotor components.